Water Dynamics Around Proteins: T- and R-States of Hemoglobin and Melittin

Marco Pezzella, Krystel El Hage, Michiel J.M. Niesen, Sucheol Shin, Adam P. Willard, * Markus Meuwly, * and Martin Karplus *

Department of Chemistry, University of Basel, Klingelbergstrasse 80, CH-4056 Basel, Switzerland

SABNP, Univ. Evry, INSERM U1204, Université Paris-Saclay, 91025 Evry, France

Department of Chemistry, MIT, USA

Department of Chemistry, University of Texas at Austin, USA

Department of Chemistry, Harvard University, USA

Laboratoire de Chimie Biophysique, ISIS, Université Louis Pasteur, 67000 Strasbourg, France

E-mail: awillard@mit.edu; m.meuwly@unibas.ch; marci@tammy.harvard.edu

Abstract

Here the abstract.

$\frac{T_0}{R_0}$

$\frac{T_0}{R_0}$

1 2

1 2

$$-\sum_{\prime}-\sum^{w}\left[\qquad\qquad\right]$$

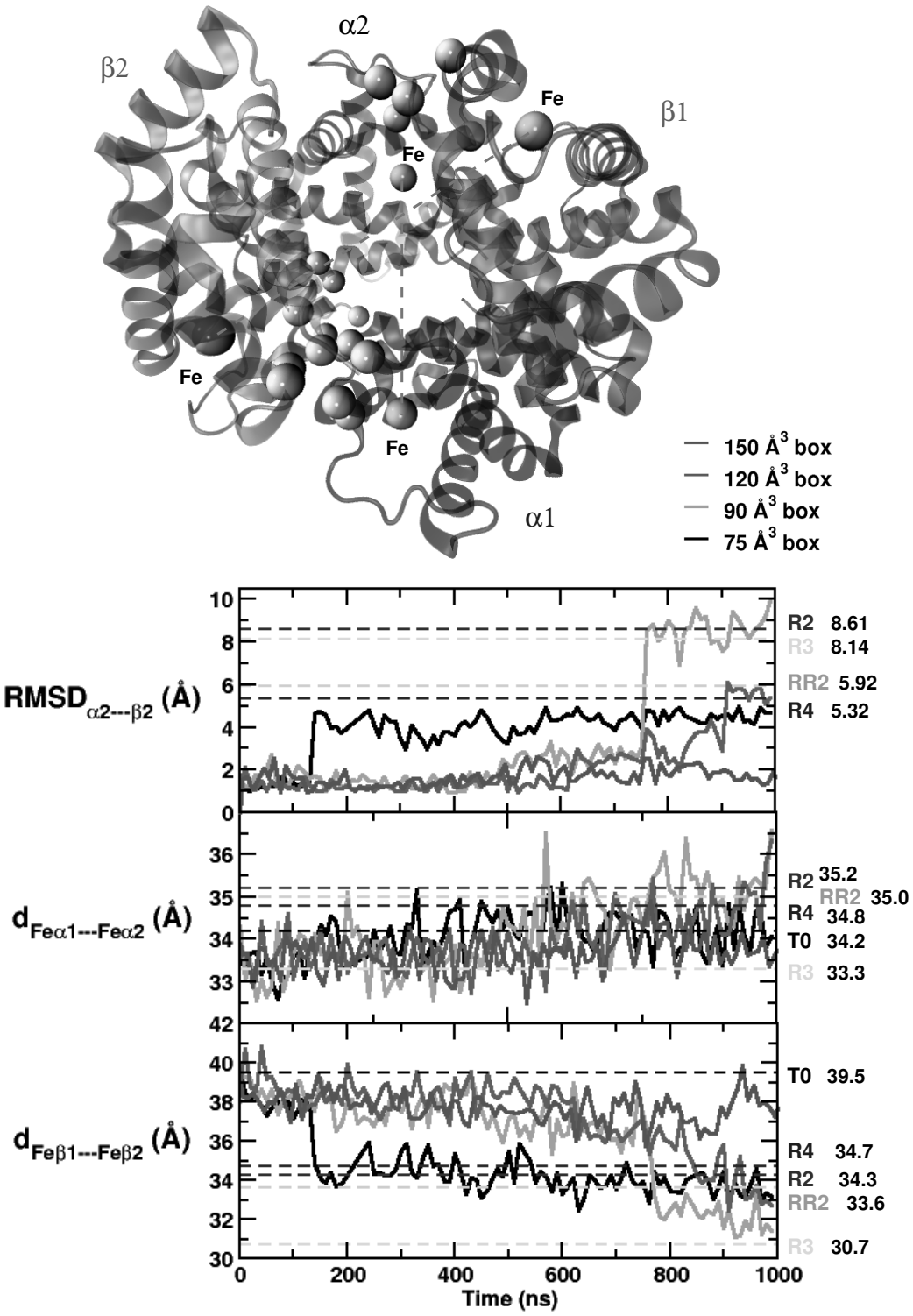
α2
β2
β1
Fe
Fe
Fe
Fe
α1
150 Å3 box
120 Å3 box
90 Å3 box
75 Å3 box
RMSDα2---β2 (Å)
R2 8.61
R3 8.14
RR2 5.92
R4 5.32
dFeα1---Feα2 (Å)
R2 35.2
RR2 35.0
R4 34.8
T0 34.2
R3 33.3
dFeβ1---Feβ2 (Å)
T0 39.5
R4 34.7
R2 34.3
RR2 33.6
R3 30.7
Time (ns)

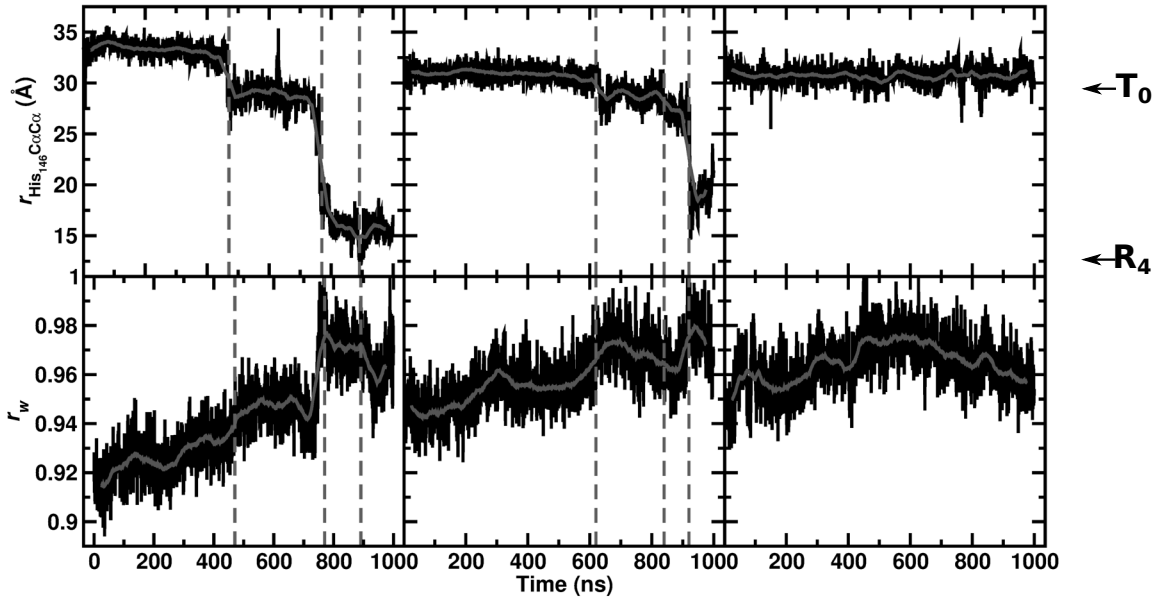

$$\frac{\text{wat}}{\text{wat}}$$

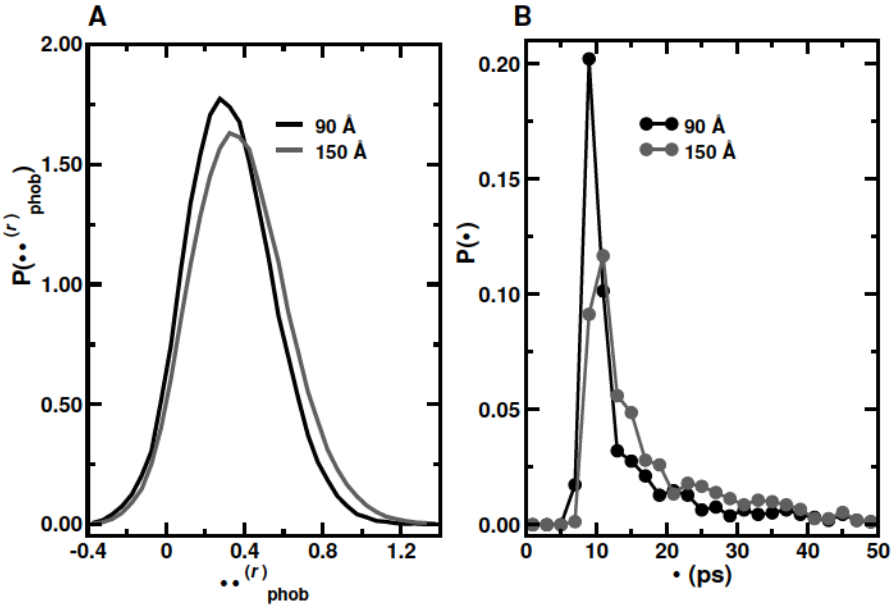

Figure 3: (**A**) The distribution of $\delta\lambda^{(r)}_{\rm phob}$ for water exposed residues of Hb in the T_0 state. The black and red lines correspond to simulations carried out in 90Å and 150Å solvent boxes, respectively. (**B**) The distribution of hydration structure relaxation times evaluated for surface residues of the T_0 state in the 90Å and 150Å simulation cell. **This figure is not sized propertly. The axes labels are too small. The panel labeling is inconsistent between the figure and the caption (capitalization)** I have redoone the figure with xmgrace, making the two graphs in the same worksheet. Please let me know if something different is needed.

of $r_w = N_{\rm wat}/N_{\rm max}$ was determined as the instantaneous number $N_{\rm wat}$ of water molecules for a specific snapshot and the maximum $N_{\rm max}$ encountered along the entire trajectory.

To obtain more detailed information, $\delta\lambda_{\rm phob}(t)$ was analyzed for the residues listed in Table 1, see Figure 4. For certain residues, structural transitions (at $t = 470$ ns, $t = 770$ ns, and $t = 891$ ns) are accompanied by abrupt rather than by gradual changes in local hydrophobicity of individual residues. Examples include Val98β_1, Thr41α_1, or Asp94α_1. By contrast, Tyr42α_1 shows a gradual decrease in $\delta\lambda_{\rm phob}$ over most of the 1 μs simulation. Except for Val98β_1 all residues that show a substantial increase in their hydrophilic ($\delta\lambda_{\rm phob} \sim 0.5$) versus hydrophobic ($\delta\lambda_{\rm phob} \sim 0$) character [Thr41$\alpha_1$, Tyr42$\alpha_1$] or a decrease [Thr38$\alpha_1$, Asp94$\alpha_1$, Asp99$\beta_2$] are at the α_1/β_2 interface. This suggests that the decay for the 90 Å box is trig-

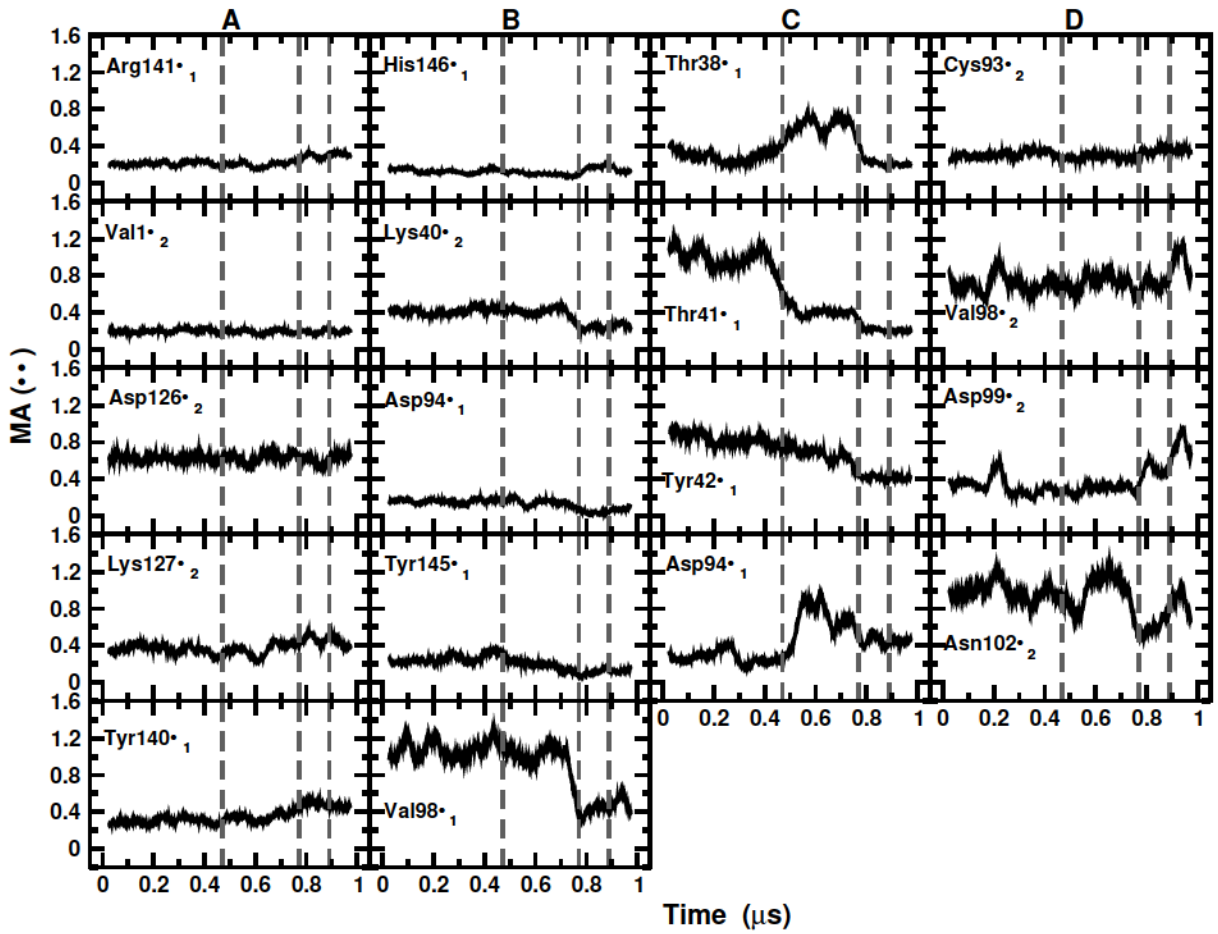

Figure 4: Local hydrophobicity for the simulation in the 90 Å box. Moving average over 50 ns of $\delta\lambda_{\text{phob}}$ as a function of time for residues involved in the C-terminal salt bridges[19] (column A), additional salt bridges (column B) and the $\alpha_1\beta_2$ shearing motion **Where is $\alpha_1\beta_2$ shearing motion described?]see p. 6** (columns C and D), see Table 1.

$\Delta\langle\delta\lambda_{\text{phob}}\rangle$ except that of Val98β_1, which is associated with the first transition (see Figure 5). Also, several of the residues at the α_1/β_2 interface show pronounced changes in local hydrophobicity that coincide with structural transitions. However, in contrast to the 90 Å box, several residues in column D (i.e., Val98β_2, Asp99β_2, and Asn201β_2) show local hydrophobicity changes that cannot be linked to a transition. For the second and third transition, there is again a clear change for Thr41α_1, Thr38α_1, and Asp94α_1. This may also suggest that the nature of the first transition (step1) in the 90 Å and 120 Å box is different. **Krystel: can we substantiate this through Figures 2, ?? to ??? Also, how about**

superimposing one $\alpha_1\beta_2$ interface and measuring the RMSD for the second pair?

Figures 2, and?? to ?? show that the transition between T_0 and R_4 occurs via intermediate structures, specifically R_2,RR_2 and R_3, via different macromolecular properties: Figure ?? shows the variation of some general properties characterizing the Hb transition, details on the His146β, that are used for characterizing the $T_0 \rightarrow R_0$ in Ref.,[4] are described in Figure ??, results on the quaternary are illustrated in Figure 2 and, finally, results for the $\alpha_1\beta_2$ interface are illustrated in Figure ??.

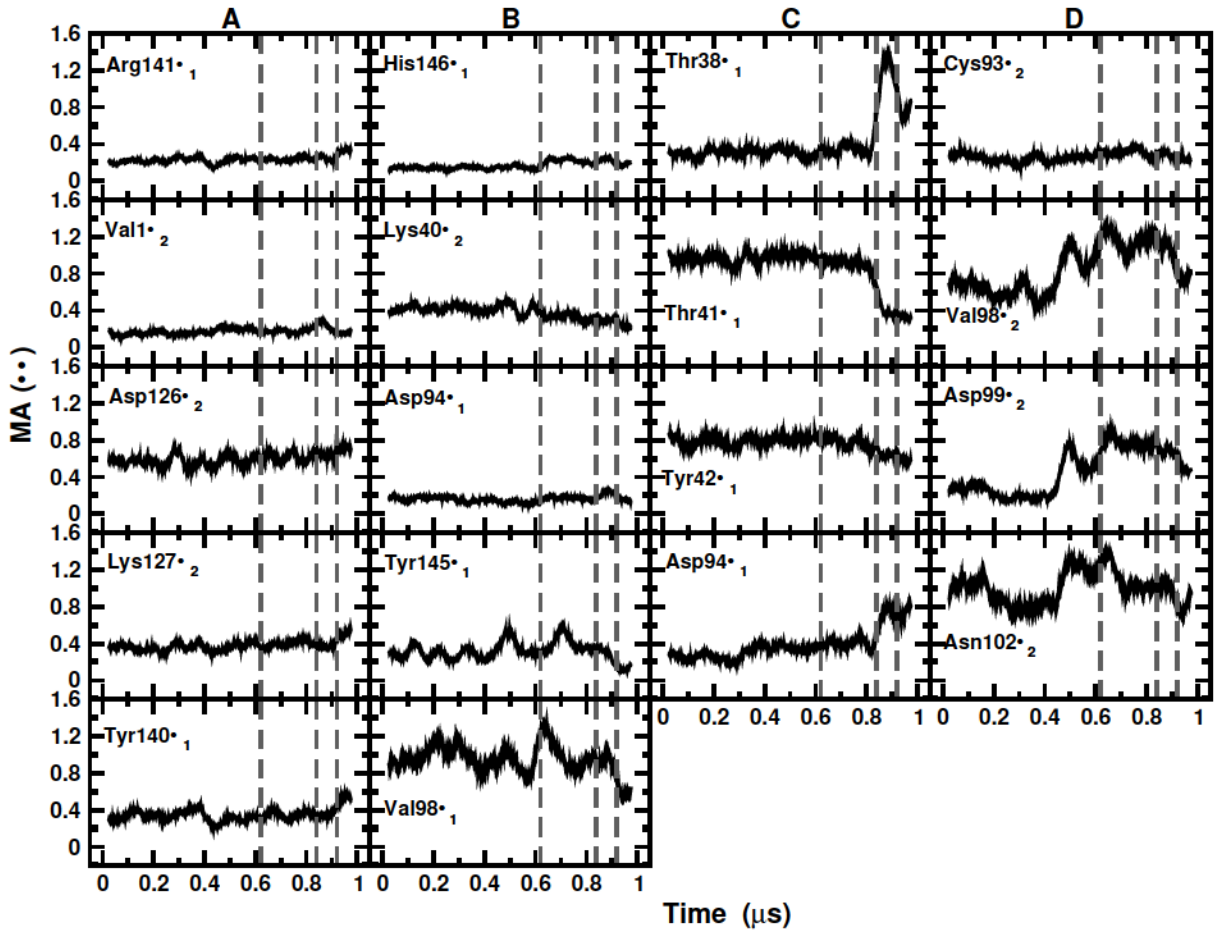

Figure 5: Local hydrophobicity for the simulation in the 120 Å box. Moving average over 50 ns of $\delta\lambda_{\text{phob}}$ as a function of time for residues involved in the C-terminal salt bridges[19] (column A), additional salt bridges (column B) and the $\alpha_1\beta_2$ shearing motion (columns C and D), see Table 1.

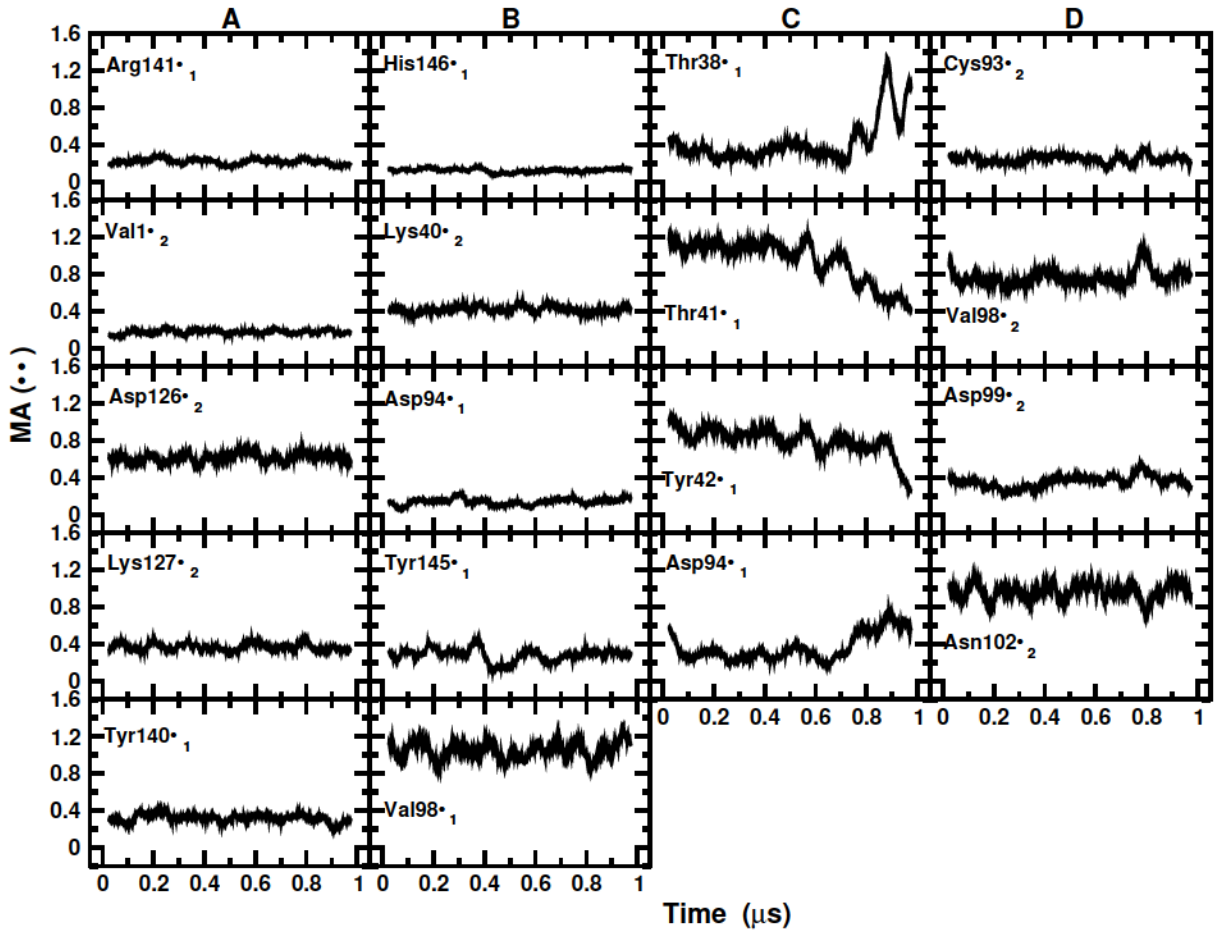

Figure 6: Local hydrophobicity for the simulation of the 150 Å box. It shows moving averages over 50 ns of $\delta\lambda_{\text{phob}}$ as a function of time for residues involved in the C-terminal salt bridges[19] (column A), additional salt bridges (column B) and the $\alpha_1\beta_2$ shearing motion (columns C and D), see Table 1.

(d) Spatio-temporal analysis based on two-dimensional correlation maps: To better understand the coupling of local hydration dynamics and the structural transitions, two-dimensional correlation maps were generated as follows. Similar to dynamic cross correlation maps (DCCMs)[22,23] for residues i and j the quantity

$$C_{ij} = \frac{\langle \Delta\delta\lambda^{(i)}_{\text{phob}} \Delta\delta\lambda^{(j)}_{\text{phob}} \rangle}{\sqrt{\langle (\Delta\delta\lambda^{(i)}_{\text{phob}})^2 \rangle \langle (\Delta\delta\lambda^{(j)}_{\text{phob}})^2 \rangle}} \tag{2}$$

was determined for each interval for which Hb was in a particular conformational state as

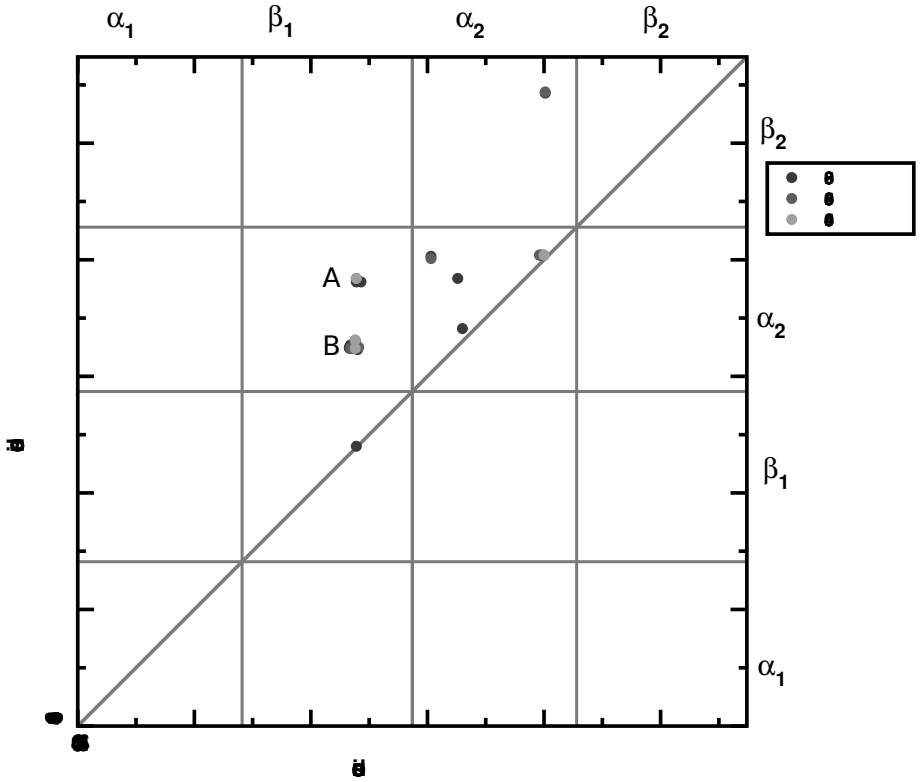
α1
β1
α2
β2
β2
α2
β1
α1
A
B

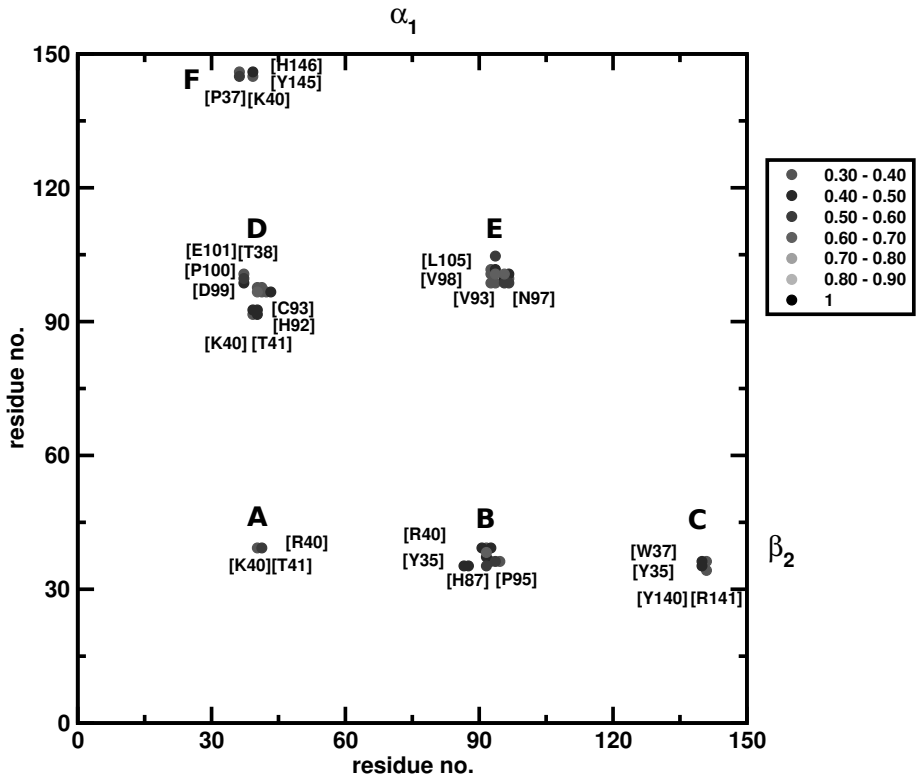
α1
150
120
90
60
30
0
residue no.
0
30
60
90
120
150
residue no.
F
[H146]
[Y145]
[P37]
[K40]
D
[E101]
[T38]
[P100]
[D99]
[C93]
[H92]
[K40]
[T41]
E
[L105]
[V98]
[V93]
[N97]
A
[R40]
[K40]
[T41]
B
[R40]
[Y35]
[H87]
[P95]
C
[W37]
[Y35]
[Y140]
[R141]
β2
0.30 - 0.40
0.40 - 0.50
0.50 - 0.60
0.60 - 0.70
0.70 - 0.80
0.80 - 0.90
1

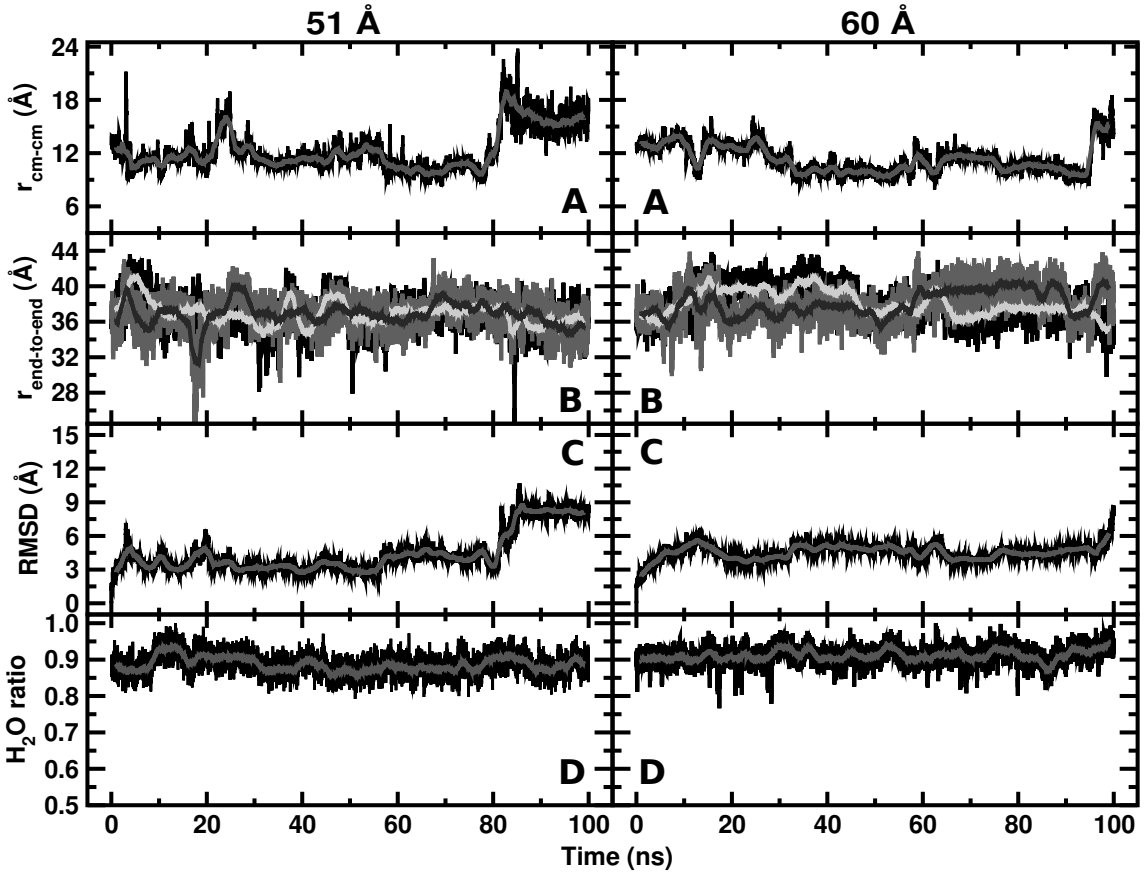
51 Å
60 Å
r_{cm-cm} (Å)
$r_{end-to-end}$ (Å)
RMSD (Å)
H_2O ratio
A
B
C
D
Time (ns)

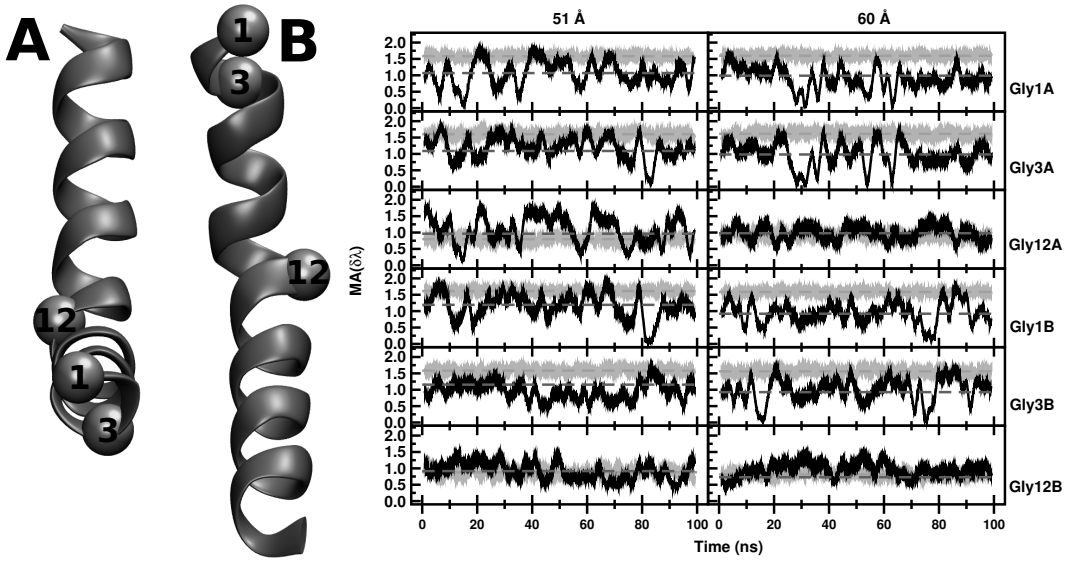
A
B
1
3
12
1
3
12
51 Å
60 Å
MA(δλ)
Gly1A
Gly3A
Gly12A
Gly1B
Gly3B
Gly12B
Time (ns)

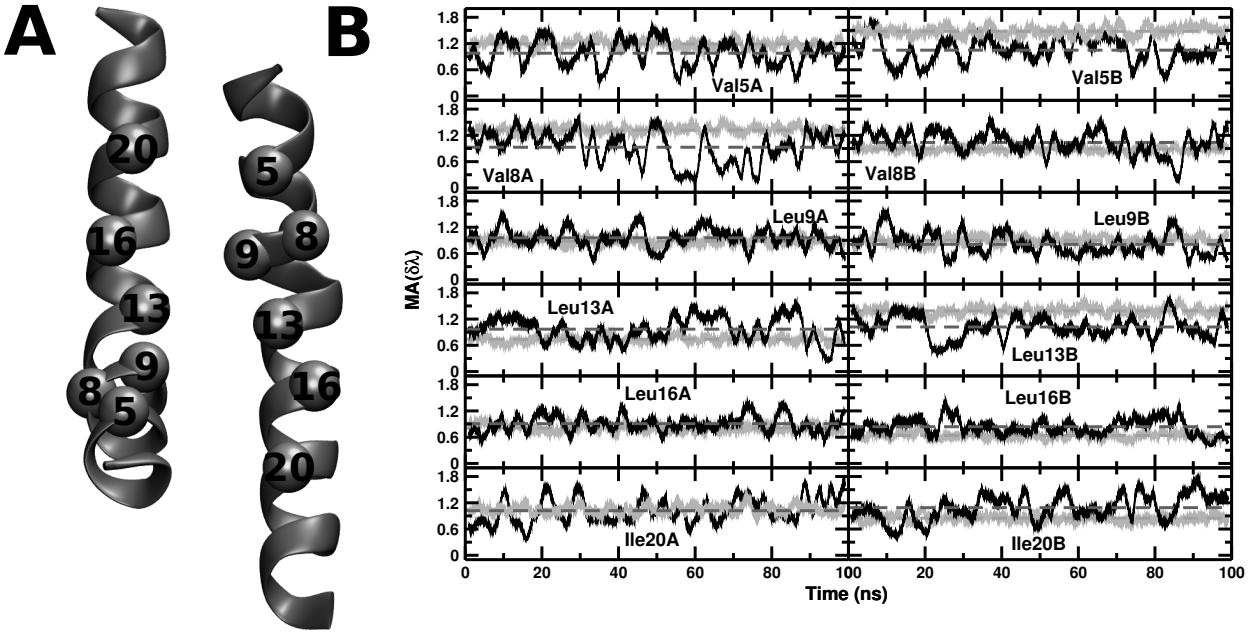
A
20
16
13
9
8
5
B
5
8
9
13
16
20
MA(δλ)
Val5A
Val5B
Val8A
Val8B
Leu9A
Leu9B
Leu13A
Leu13B
Leu16A
Leu16B
Ile20A
Ile20B
Time (ns)

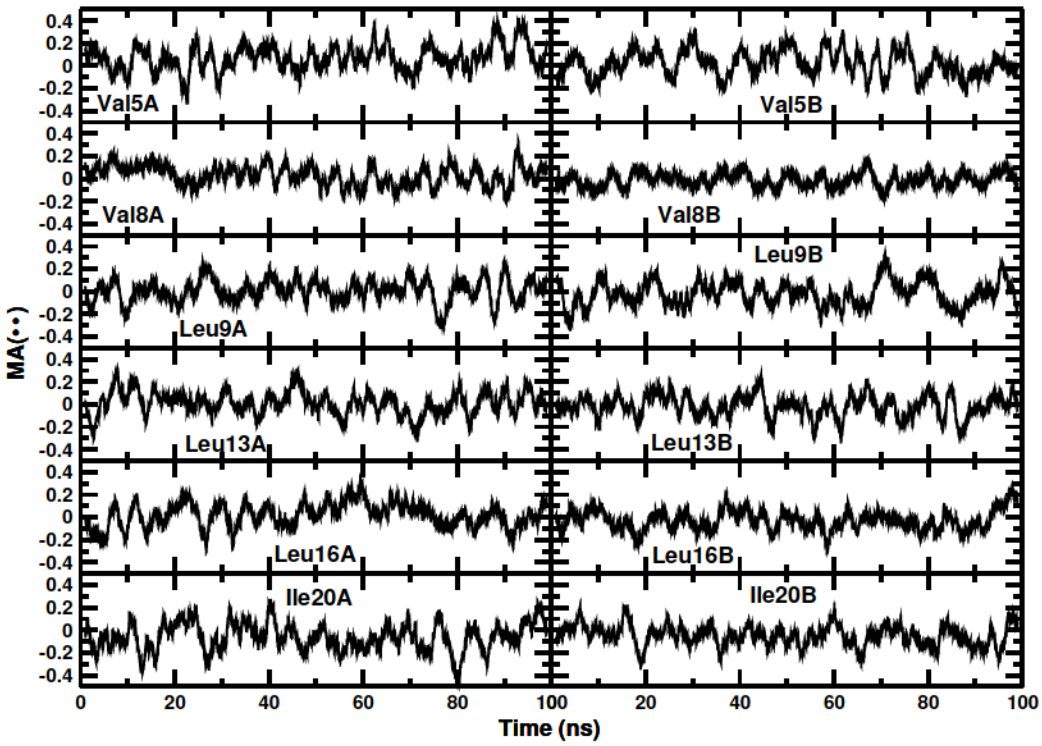

Figure 12: Difference in hydrophobicity for the residues in the melittin dimer hydrophobic pocket (residues Val5, Val8, Leu13, Leu16, Ile20) for the rigid simulations in the 51 and 60 Å boxes. The data reported is $\Delta\delta\lambda = \delta\lambda_{60} - \delta\lambda_{51}$, i.e. the change in LH from the simulation in the two water boxes. The change in $\Delta\delta\lambda_{\text{phob}}$ due to the box size is up to 40%.

the chains (from Val5 to Leu16) is highlighted by the lower $\delta\lambda$ (of 0.1-0.2 units) compared with the C- and N-terminal parts.

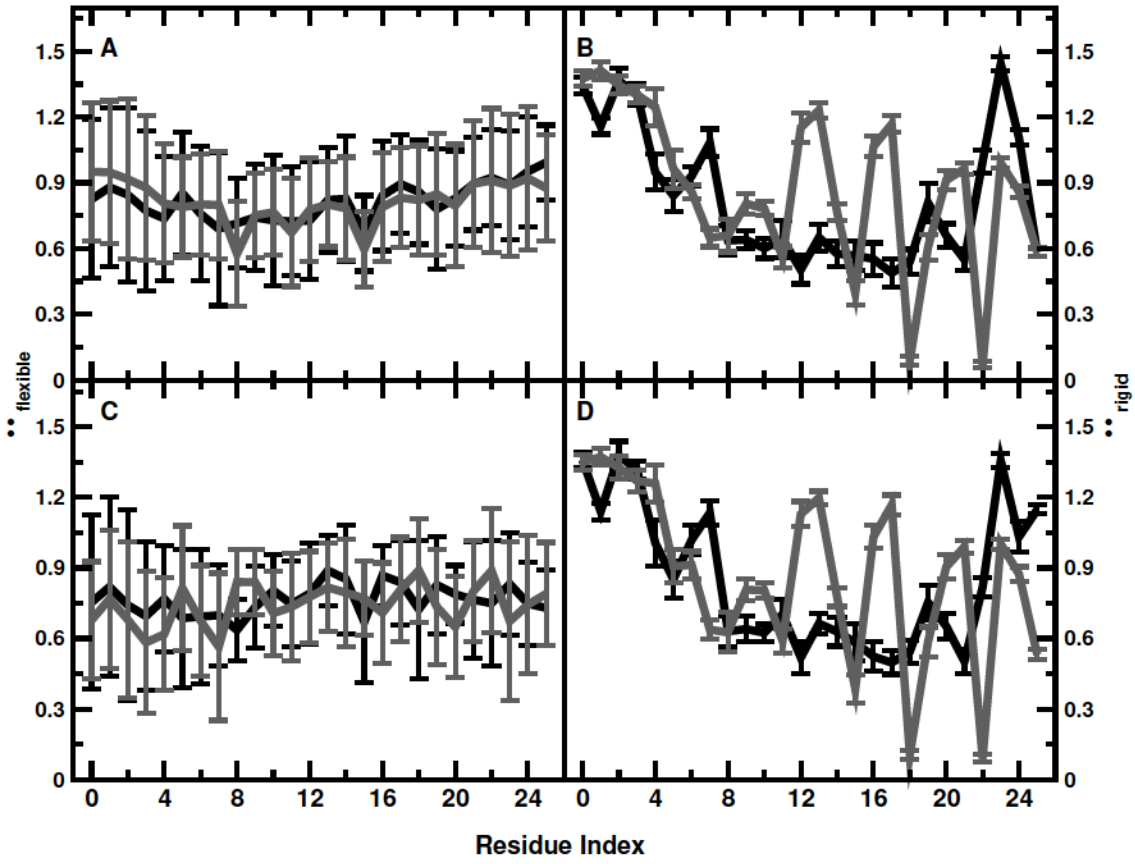

Figure 13: Average $\delta\lambda$ per residue for the 100 ns for chains A (black) and B (red) for flexible (panels A and C) and rigid (panels B and D) melittin dimer. The top row is for the 51 Å box and the bottom row for the 60 Å box. The value of the LH ranges from $0.50 < \delta\lambda < 1.00$ for the flexible dimer and between $0.00 < \delta\lambda < 1.50$ for the rigid dimer. For the rigid dimer, the central part of the A-helix has consistently lower values of LH compared with the C- and N-terminal parts. For chain B larger variations in LH are found for some of the residues due to its different structure. The periodicity of the red traces (panels B and D) reflects the helical structure which is apparent for monomer B but less so for monomer A. For flexible melittin the variation of LH along the sequence is much smoother than for rigid melittin as a consequence of dynamical averaging. [**Any reason for this?**].**described in text.**

The average hydrophobicity per residue is illustrated in Figure 13. The main difference between simulations of the flexible (left) and rigid (right) melittin dimer is the amplitude of the fluctuation of the hydrophobicity, but not its sign. Simulations of rigid melittin in the

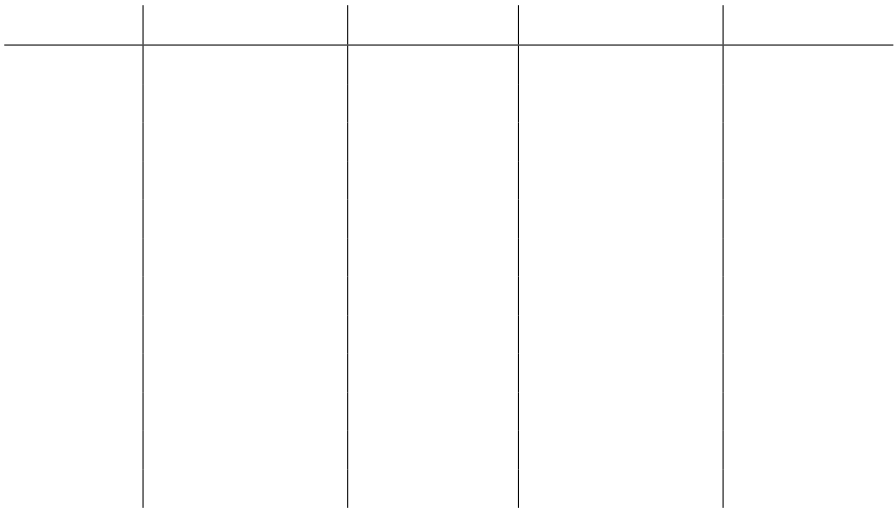

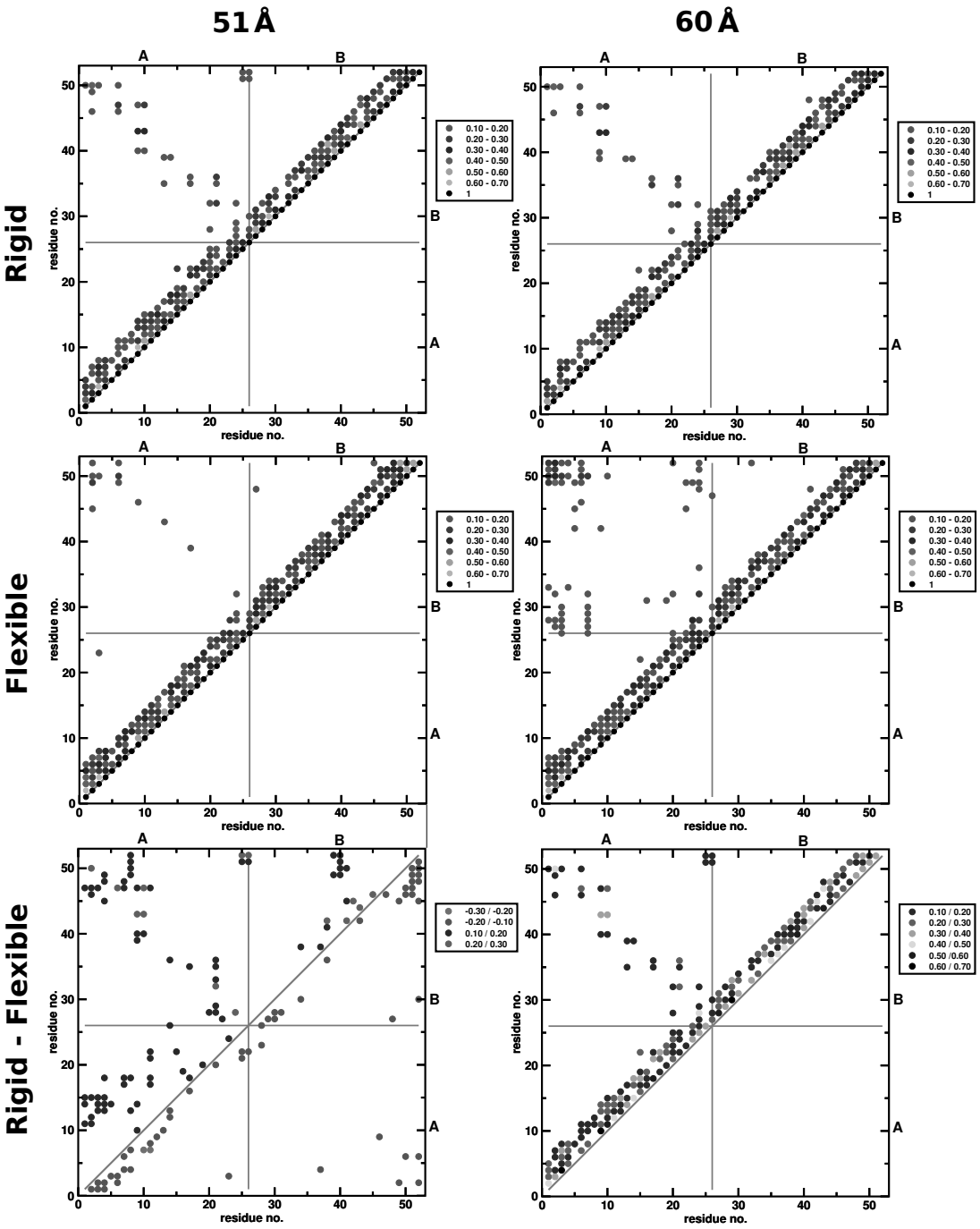
51 Å
60 Å
Rigid
Flexible
Rigid - Flexible
residue no.
A
B
0.10 - 0.20
0.20 - 0.30
0.30 - 0.40
0.40 - 0.50
0.50 - 0.60
0.60 - 0.70
1
-0.30 / -0.20
-0.20 / -0.10
0.10 / 0.20
0.20 / 0.30
0.30 / 0.40
0.40 / 0.50
0.50 /0.60
0.60 / 0.70

Nature *230*

PLoS Comput

Biol *6*

J. Phys. Chem. B *116*

7

8

8

Nature *392*

J. Biol. Chem. *257*

J. Biol. Chem. *257*

Nature *392*

J. Chem. Theor. Comput. *14*

J. Comput. Chem. *30*

J. Chem. Theor. Comput. *8*

J. Biol. Chem. *255*

The Journal of Chemical Physics *103*

Mol. Phys. *34*

J. Phys. Chem. B *122*

J. Phys. Chem. B *114*

Nature *228*

J. Mol. Biol. *360*

Biochemistry *44*

Prot. Struct. Funct. Genom. *11*

J. Mol. Biol. *263*